UROP - Helium Turbine Preliminary Modelling

Shail Desai
sd718@cam.ac.uk
King's College

August 17, 2018

1 Introduction

The initial project objective was to model, with reasonable accuracy, the operating conditions and output behaviour of the Helium Turbine for use in the SABRE Engine. Table 1 contains relevant physical quantities and fixed parameters about which the design space was to be mapped. Starred Items indicating assumed values.

Quantity/Parameter	**Value**	**units**
P_{0in}	145	bar
T_{0in}	950	K
Work Output (W_{out})	17	MW
Mass Flow Rate ($\dot{m}$)	16	kg/s
Shaft Rotation Speed (Ω)	6782	rpm
C_p	5190	J/K
γ	1.667	-
ρ_{in}	7.6	kg/m^3
R	2080	
$Reaction^*$	50	%
μ	31×10^{-6}	Ns/m^2

Table 1: Physical Constants and Fixed Parameters

2 Basic/Preliminary Calculations

The key design variables to set the Turbine characteristics were selected as Flow Coefficient (ϕ), Stage Loading (ψ), Reaction (Λ) and the Number of Stages (n_{stages}). Out of these the Reaction was set initially at 50% while the others were left floating. The Blade Aspect Ratio (AR) was later introduced for the loss calculations.

2.1 Sizing and Velocity Triangles

Initial Calculations involved simply mapping the variation of the Turbine Mean Radius (r), Axial Flow Velocity (V_x), Blade Span at Inlet (H_{in}) and Mean Blade Speed (U) with the three floating variables. The Mean Radius and Axial Flow Velocity were assumed constant across the turbine The relevant formulae were:

$$r_{mean} = \frac{Wout}{\sqrt{\dot{m}\psi\Omega^2 \times n_{stages}}}$$

$$V_x = \Omega r_{mean}\phi$$

$$H = \frac{\dot{m}}{\rho 2\pi r_{mean} V_x}$$

$$U = \Omega r_{mean}$$

$$C_x = H/AR$$

In addition to the above quantities, the 50% reaction meant that the flow Velocity Triangles would be symmetric as well as repeating over the turbine stages. The flow angles (α being absolute angles and β being relative angles) were subsequently calculated as:

$$\alpha_1 = tan^{-1}(\frac{1-0.5\psi-\Lambda}{\phi})$$

$$\beta_3 = tan^{-1}(tan(\alpha_1) - \frac{1}{\phi})$$

$$\beta_2 = tan^{-1}(tan(\alpha_2) - (1./\phi))$$

$$\alpha_3 = \alpha_1;$$

$$\alpha_2 = -\beta_3$$

$$\beta_1 = \beta_3$$

The flow angles were then used to calculate the absolute and relative flow velocities across a stage from V_x.

The variation of the above quantities with the floating variables can be seen in the figures below.

2.2 Operating Point Contours (against ϕ and ψ)

For the following contour plots, the number of stages was fixed at 12 and blade span values plotted are those at the turbine inlet.

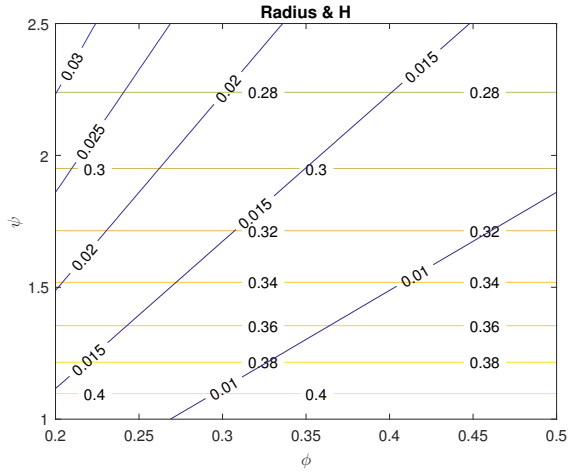

Figure 1: Radius(yellow) and Span(blue) in m

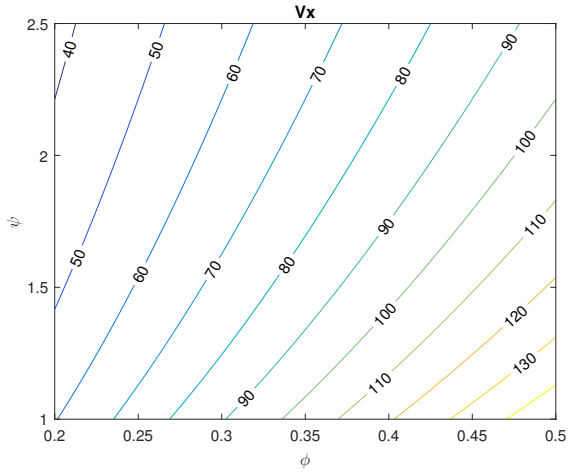

Figure 2: Axial Velocity in m/s

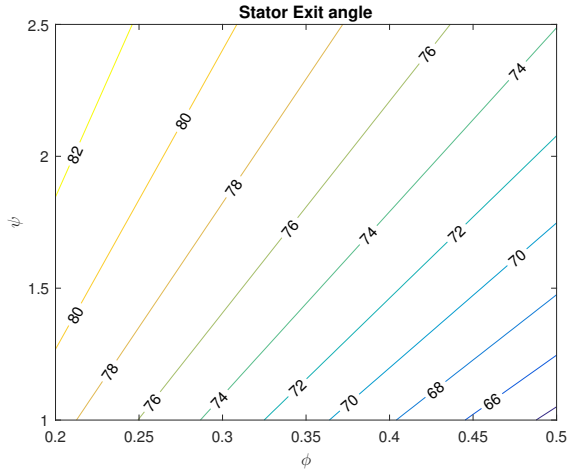

Figure 3: $\alpha_2(deg)$

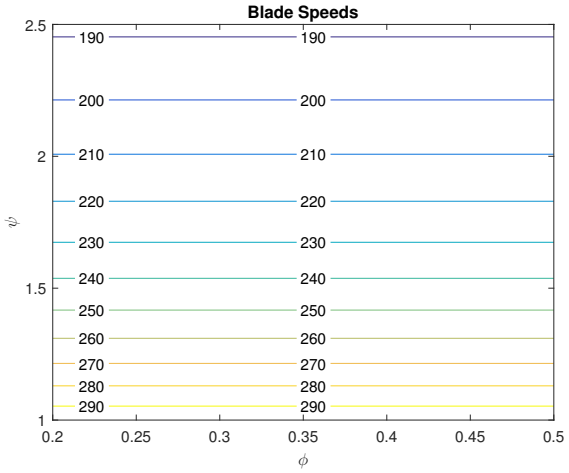

Figure 4: Blade Speeds (m/s)

From the formula used is evident that the mean radius is simply a function of, and inversely related to ψ. This is supported by Fig. 1, with the contour spacing increasing with higher Stage Loading indicative of the inverse square root relation. The constant mass flow (continuity) condition also results in an inverse relationship between the mean radius and blade span. However, the dependence of the span on V_x adds an additional inverse relationship with ϕ as well. This is also evident from Figs 1 and 2. Higher Stage Loading requires a larger flow turning is also supported by the increasing relationship between ψ and α_2, while as expected, a greater Axial Velocity, arising from a larger Flow Coefficient would reduce the flow turning, resulting in the inverse relationship with ϕ.

2.3 Gas Properties

The planned modelling required certain quantities to be calculated at each stage. A starting assumption for this was that the stagnation enthalpy drop across all stages was equal, i.e the stagnation enthalpy and temperature drop across a stage were calculated as:

$$\Delta h_0 = \frac{\psi \, r_{mean}^2 \Omega^2}{n_{stages}}$$

$$\Delta T_0 = \Delta h_0 / c_p$$

Isentropic equations were used to calculate the (static and stagnation) Temperatures, Pressures and the density at each stage exit. The stage-to-stage density ratio was then used to calculate the span variation across all the stages. The static temperature was also used to calculate the stage exit Mach numbers (absolute and relative). The current calculations neglect the effects of the losses, except in the calculation of the efficiency.

3 Loss Models

For modelling the losses in the turbine, the blade aspect ratio (AR) was added as an additional parameter. From this, and the blade spans, the chord lengths at each stage were calculated. The flow Reynold's Number at each stage was also calculated as:

$$Re_x = \rho V_2 C_X / \mu$$

3.1 Profile Loss

Additional values required for the profile loss included the Zweifel (lift) Coefficient Z, assumed as 0.8[2], the blade local Dissipation Coefficient C_d, taken as $0.002 \times (\frac{Re}{500000})^{-0.2}$, and the ideal fractional change in velocity for the blade surface $\frac{\Delta V}{\overline{V}}$, taken as $\sqrt{3}$. The blade pitch p (at the stator, and assumed identical for the rotor given the 50% reaction) and throat width w were then calculated as:

$$p = \frac{0.5Z \times C_x}{cos^2(\alpha_2)(|tan(\alpha_1) - tan(\alpha_2))}$$

$$w = p \times cos(\beta_2)$$

The entropic loss coefficient $\zeta_{profile}$, for the stage, i.e including losses across the stator and rotor blade rows, was then calculated, using Denton (1993), as:

$$\zeta_{profile} = C_d(2\frac{\overline{V}}{\Delta V} + 6\frac{\Delta V}{\overline{V}})(|tan(\alpha_2) - tan(\alpha_1)| + |tan(\beta_3) - tan(\beta_2)|)$$

and converted to a specific entropy rise $\Delta s_{profile}$ at each stage by multiplying it by $0.5V^2/T$.

3.2 Trailing Edge Loss

The trailing edge loss was also modelled using the relationships in Denton (1993). The base pressure coefficient C_{pb} was taken as -0.15, and the trailing edge thickness t_{TE} as 1mm. The boundary layer dissipation term $\frac{2\theta}{w}$ was neglected, as their effects were sufficiently accounted for in the profile loss. To calculate δ^*, $\zeta_{profile} = 2\theta/w$ was used, along with an assumed shape factor of 1.4 for a turbulent boundary layer. ζ_{TE} was therefore calculated as:

$$\zeta_{TE} = 2 \times (-C_{pb}t_{TE}/w + ((t_{TE} + \delta^*)/w)^2)$$

and converted to an entropy rise the same way as the Profile Loss Coefficient. Note the factor of two to account for both blade rows in a stage.

3.3 Endwall Scrubbing Losses

The relationships in Denton (1993) were once again used to estimate the Endwall losses. The wall dissipation coefficient C_{Dwall} was taken as 0.002 and the loss was split into three components for the flow over a quarter-chord length at stage entry, a quarter-chord length at stage exit, and a chord length between the stator and rotor blade rows. The three constituent entropy rises for a stage were calculated as:

$$\text{Stage Entry: } 2 \times \rho\, C_{Dwall} V_1^3\, 2\pi r \times 0.25C_x/T$$

$$\text{Stator to Rotor: } 2 \times \rho\, C_{Dwall}(V_2^3 + V_{2rel}^3)2\pi r \times 0.25C_x/T$$

$$\text{Stage Exit: } 2 \times \rho\, C_{Dwall} V_3^3\, 2\pi r \times 0.25C_x/T$$

Note the additional factor of 2 applied to account for the hub and the casing. These were then summed to generate a total entropy rise from endwall scrubbing for a given stage.

3.4 Secondary Flow Calculations

The relationship used for the stagnation pressure loss coefficient due to secondary flows Y_{sec} included a slight modification from [1] on Dunham & Came(1970)'s prediction. In addition to this the vector mean air angle α_m had to be calculated using Sharma and Butler(1986)'s The formula used therefore was:

$$\alpha_m = -cot^{-1}[0.5\ (cot(\alpha_1) + cot(\alpha_2))]$$

$$Y_{sec} = 2 \times 0.375 \times 0.1336\ \frac{C_x}{H}\frac{cos^3(\alpha_2)}{\sqrt{cos(\alpha_1)}}\frac{(tan(\alpha_1)-tan(\alpha_2))^2}{cos(\alpha_m)}$$

$$\Delta s_{sec} = Y_{sec}(h_0 - h)/T$$

Note the factor of 2 to account for both blade rows

3.5 Tip Clearance Losses

Relationships from Denton(1993) were used for both shrouded and unshrouded blades.

3.5.1 Shrouded Blades

The relationship used assumes no change in swirl across the seal and no loss suffered by the leakage flow until it reaches the throat of the jet. The contraction coefficient was taken as 0.6, and with V_x held constant, the fractional leakage mass flow across a blade row was calculated as:

$$\frac{m_L}{m_m} = \frac{gC_c}{H}\sqrt{sec^2(\alpha_2) - tan^2(\alpha_1)}$$

For calculations across the rotor, the absolute flow quatities (angles and velocity) were replaced by their relative counterparts. The fractional leakages were converted to entropy rises using:

$$\Delta s_{tip} = \frac{m_L}{m_m}V_2^2(1 - \frac{tan(\alpha_1)}{tan(\alpha_2)}sin^2(\alpha_2))$$

As before, absolute flow quantities were replaced by their relative counterparts for calculations across the rotor.

3.5.2 Unshrouded Blades

For calculations involving unshrouded blades, Denton (1993) suggests assuming the blade suction side and pressure side local velocity ratios V_s/V_2 and V_p/V_2 to be 1 and 0,3 respectively. This set the integral term in Denton (1993):

$$\int_0^1 (\frac{V_s}{V_2})^3(1 - \frac{V_p}{V_s})\sqrt{(1 - (\frac{V_p}{V_s})^2)}\frac{dz}{C_x} = 0.65.$$

The entropy rise was then calculated as:

$$\Delta s_{tip} = \frac{C_{dtip}\ g\ C_x}{Hp\ cos(\alpha_2)} \times 0.65$$

4 Efficiency Calculation

The relevant entropy rises for each stage summed, and the following total entropy rises at each stage were further summed to obtain a total entropy rise across the turbine. This was then multiplied by the exit static temperature T_{out} to obtain an enthalpy change h_{loss}.

The total-to-total efficiency of the turbine η_{tt} was calculated as :

$$\eta_{tt} = \frac{\Delta h_{0s}}{\Delta h_{0s} + h_{loss}}$$

In addition to the isentropic efficiency, the lost work ratios due to each loss mechanism was calculated as follows (using the profile loss as an example):

$$\eta_{profile} = \frac{T_{out} \Delta s_{profile}}{\Delta h_0}$$

5 Results

For the following results, out of ψ, ϕ, n_{stages} two were fixed at arbitrarily chosen values, while the third was swept through. A evenly spaced set of Aspect Ratios was also fed in as an array. Reaction was fixed at 0.5.

5.1 Result Variation with n_{stages}

For the following graphs $\phi = 0.45$, and $\psi = 2.4$.

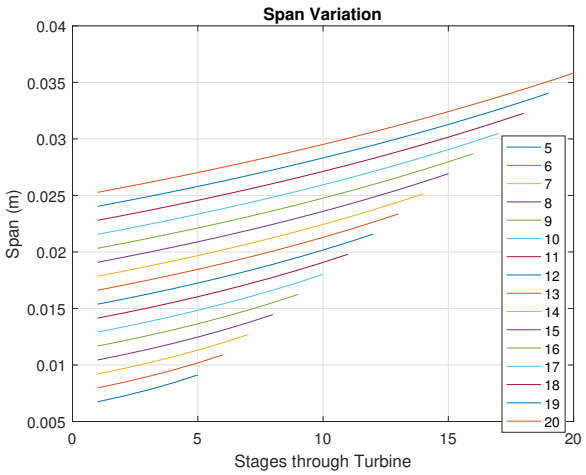

Figure 5: Span Variation across Turbine

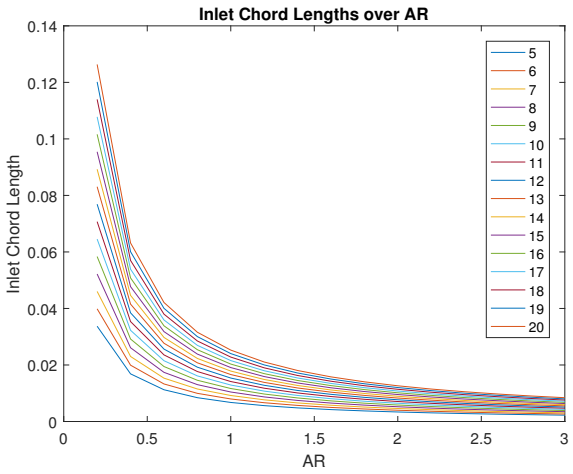

Figure 6: Inlet Chord Variation with AR

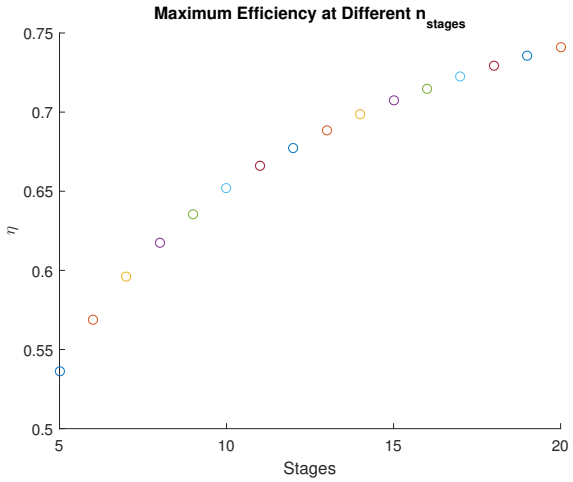

Figure 7: Maximum Efficiency Variation

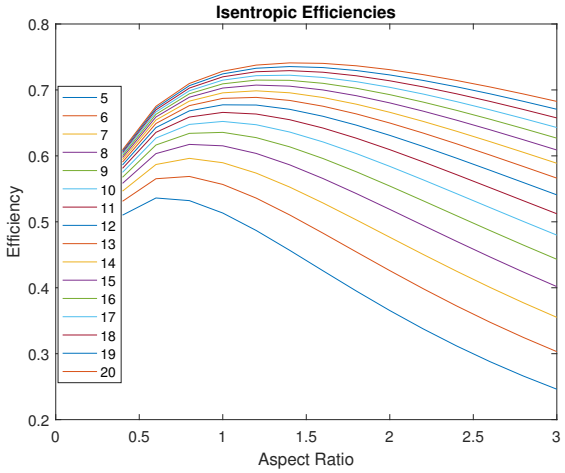

Figure 8: Isentropic Efficiencies

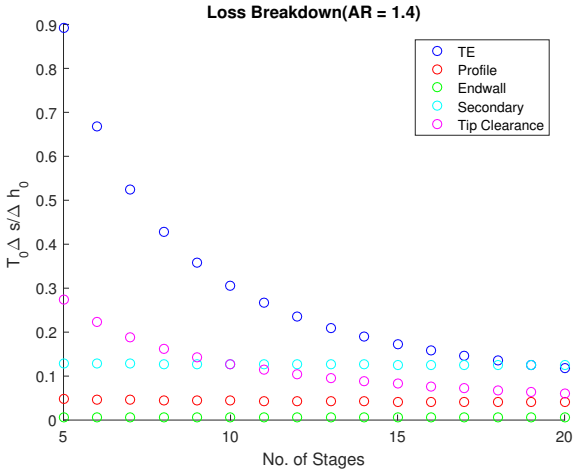

Figure 9: Lost Efficiency Breakdown and Variation

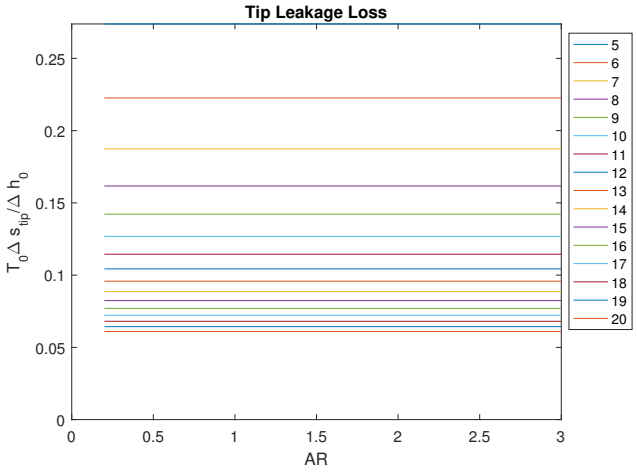

Figure 10: Tip Losses

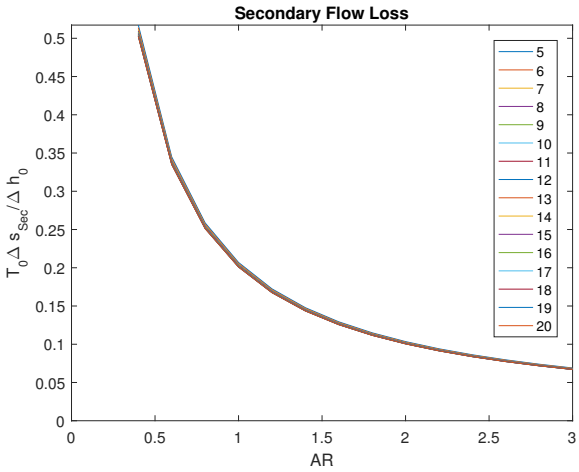

Figure 11: Secondary Flow Losses

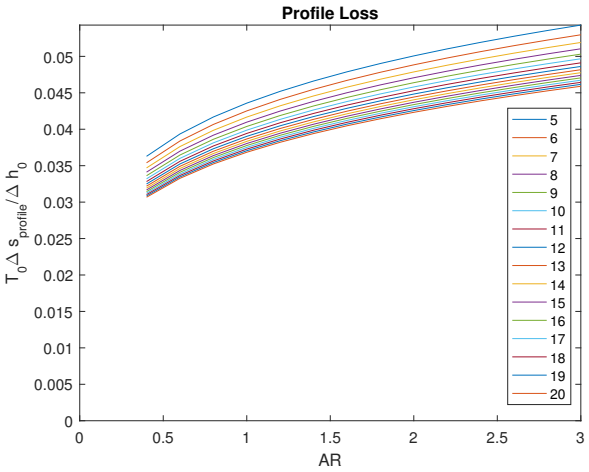

Figure 12: Profile Losses

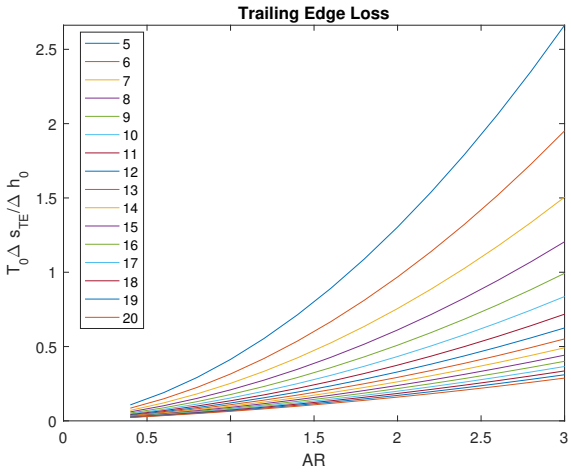

Figure 13: Trailing Edge Losses

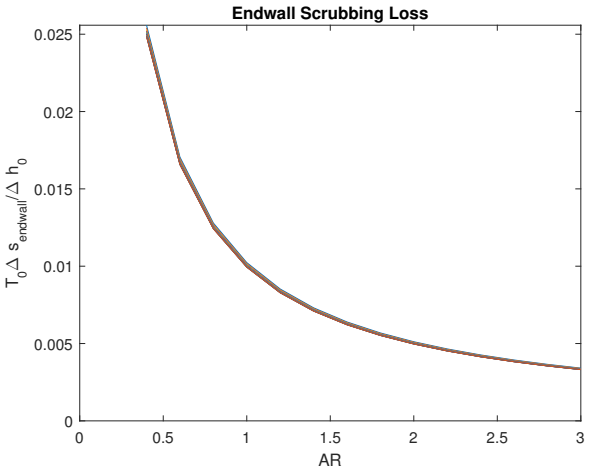

Figure 14: Endwall Scrubbing Losses

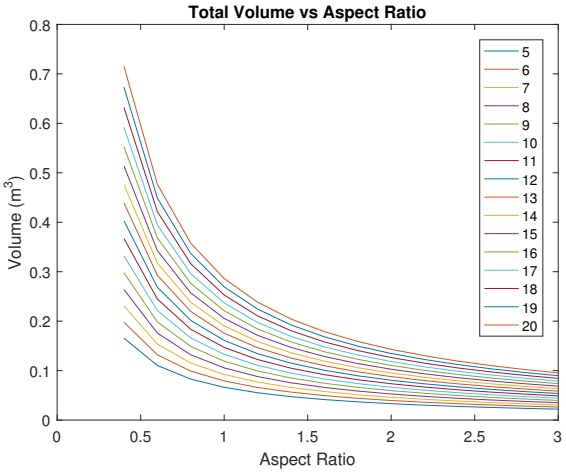

Figure 15: Total Volume Variation

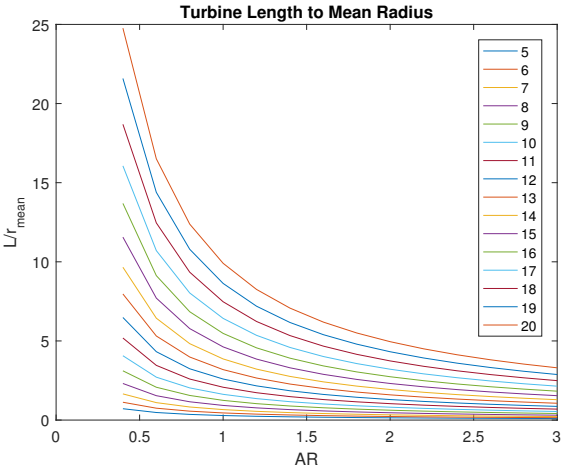

Figure 16: Turbine Length to Mean Radius

The overall efficiency seem to push towards a higher number of stages with an optimal Aspect Ratio of increasing from 0.6 at 5 stages to 1.7 at 20 stages.
The dependancy on AR can be seen in the individual loss variation charts. While Tip Losses are independent of AR, TE losses increase strongly with AR, due to the increasing t_{TE}/w ratio. This is compounded at lower values of n_{stages}, where the smaller spans further reduced the Chord and consequentially the throat width. The Profile losses also increase with AR, due to the Reynold's Number Variation

The reduction in C_x with AR resulted in the corresponding decrease in Secondary and Endwall Scrubbing Losses. However the small relative magnitude of these losses compared to the TE and tip losses at low n_{stages} placed the optimal AR (at the given ϕ and ψ values) at quite a low value.

The magnitudes of both the Secondary and the Endwall Scrubbing losses relative to the other losses increases with a higher number of stages, due to the drop in the Tip Leakage (due to greater Span/Tip clearance ratios at higher n_{stages}) and TE losses. This pushes the optimal AR to higher values for higher n_{stages}.

5.2 Result Variation with ψ

For the following graphs $\phi = 0.45$, and $n_{stages} = 12$.

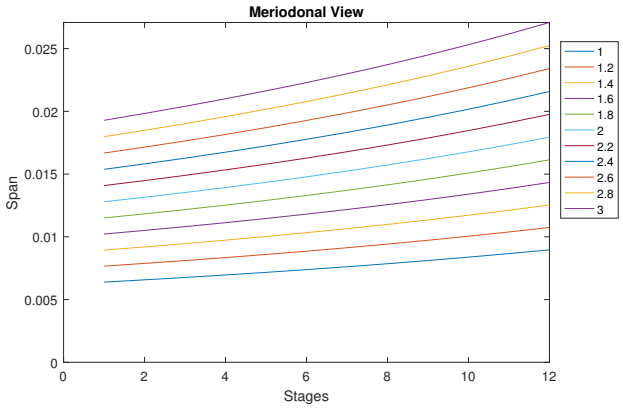

Figure 17: Span Variation across Turbine

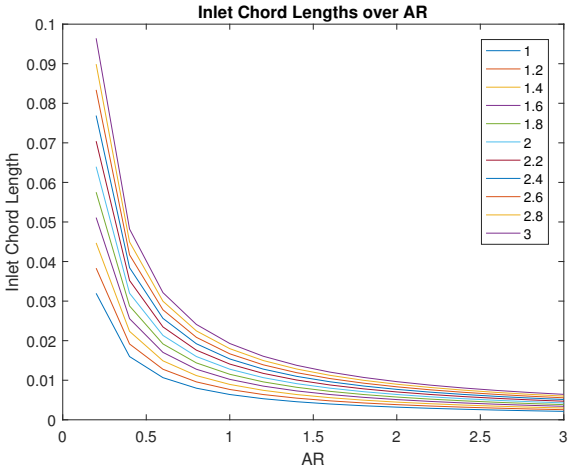

Figure 18: Inlet Chord Variation with AR

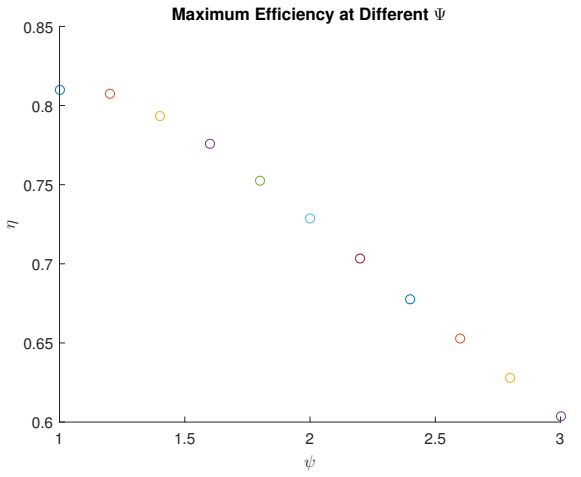

Figure 19: Maximum Efficiency Variation (at optimal AR)

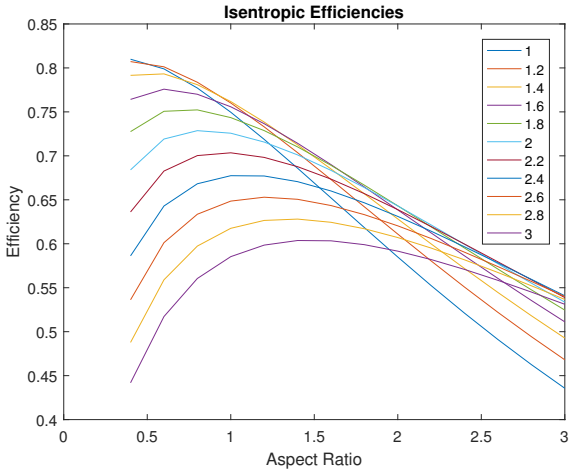

Figure 20: Isentropic Efficiencies

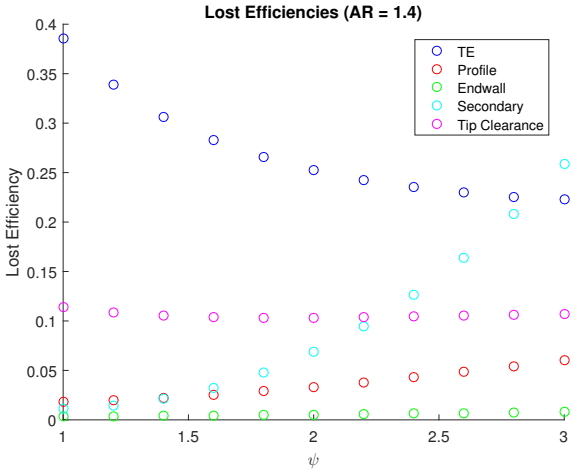

Figure 21: Lost Efficiency Breakdown and Variation

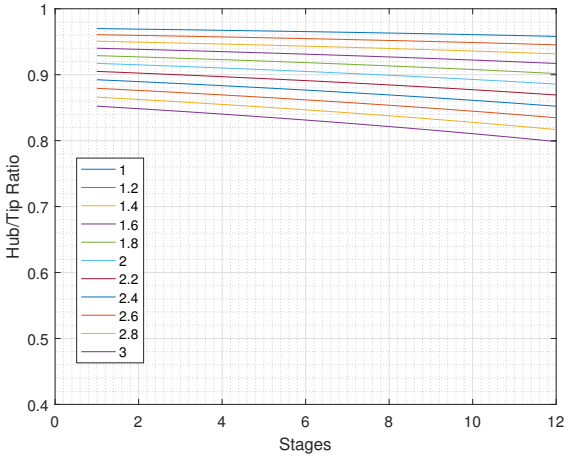

Figure 22: Hub to Tip Ratio Variation

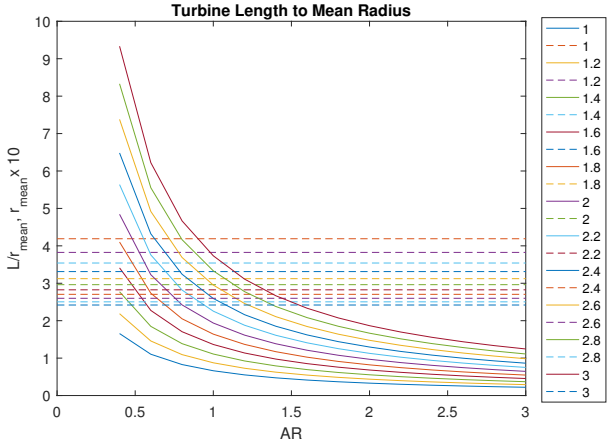

Figure 23: Turbine Length to Mean Radius

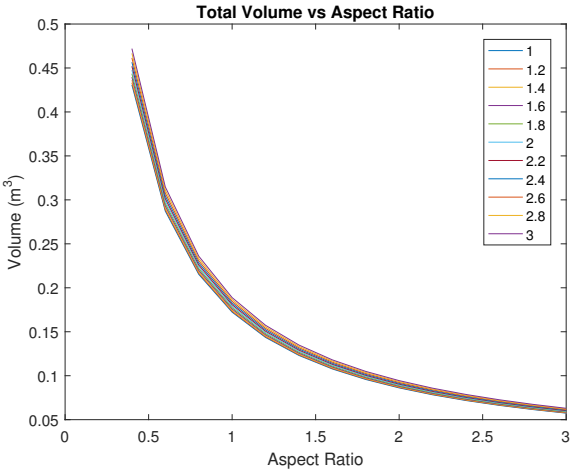

Figure 24: Volume Variation with AR

The main features to investigate are the optimal value for $\psi = 1$ and lost efficiency breakdown plot.

The model pushes towards the optimal ψ value. The optimal AR is as low as possible at low ψ, rising to 1.5 at high ψ. The lost efficiency breakdown graph provides some insight as to the cause for the optimal ψ; above certain loadings, the decreasing TE losses are surpassed by the other losses, all of which increase with ψ. Increasing ψ would reduce the radius and therefore increase the Span, driving down the t_{TE}/w and Span to Clearance ratios, reducing TE and Tip Leakage losses respectively. However, increasing the Stage Loading also greatly increased the flow turning, which offset the effect of the increasing span for the Tip Clearance losses, resulting in an initially decreasing plot that flattens out. The flow turning increase also results in a sharply increasing Secondary Flow loss curve, despite the increasing span. Increasing the span, and consequently, chord, also increased the Profile Losses and marginally increased the Endwall Scrubbing losses by increasing the Axial length of a single stage. The Profile losses also increase due to the increased flow velocities at higher ψ.

Therefore, at low ψ, where the TE and tip clearance losses dominate, the optimal AR is as low as possible to minimise the TE losses. At high ψ, the optimal AR rises to minimise the now-large Secondary Losses.

5.3 Result Variation with ϕ

For the following graphs using the information deduced from the previous results, it was thought beneficial to change the fixed parameters so that $n_{stages} = 20$, and $\psi = 1.0$.

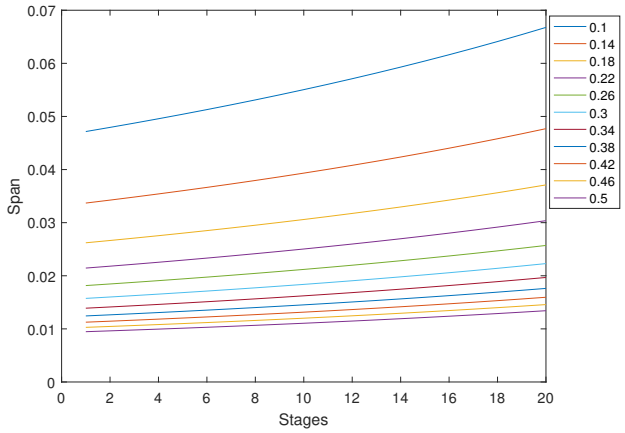

Figure 25: Span Variation across Turbine

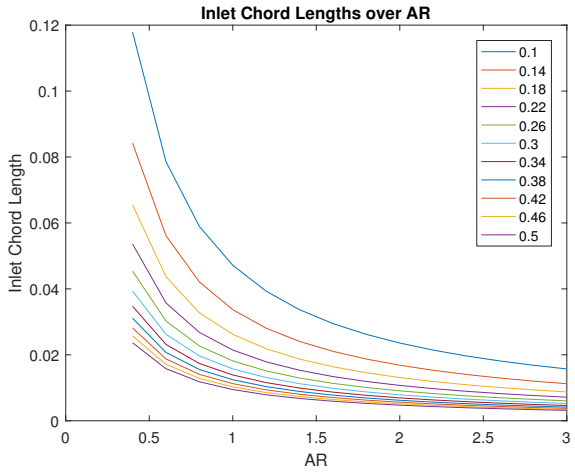

Figure 26: Inlet Chord Variation with AR

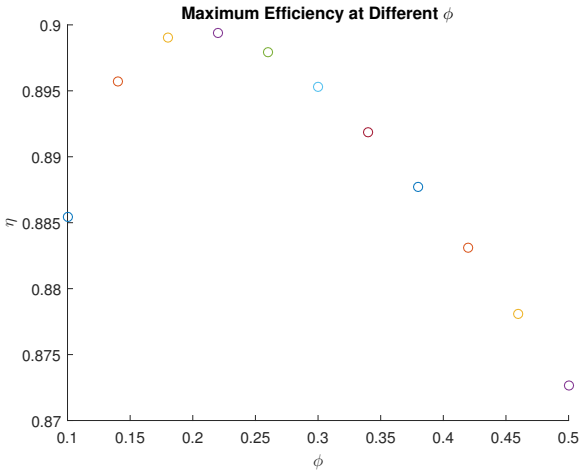

Figure 27: Maximum Efficiency Variation

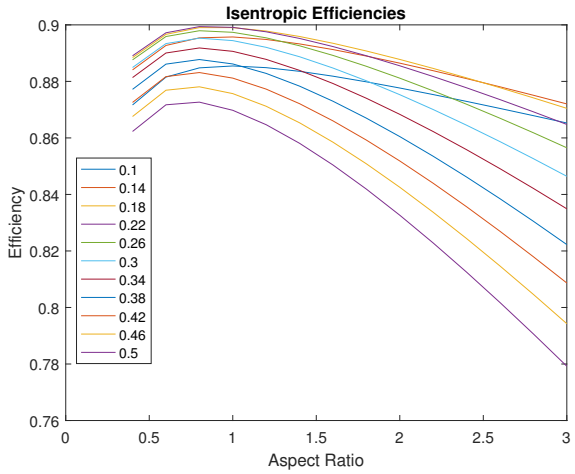

Figure 28: Isentropic Efficiencies

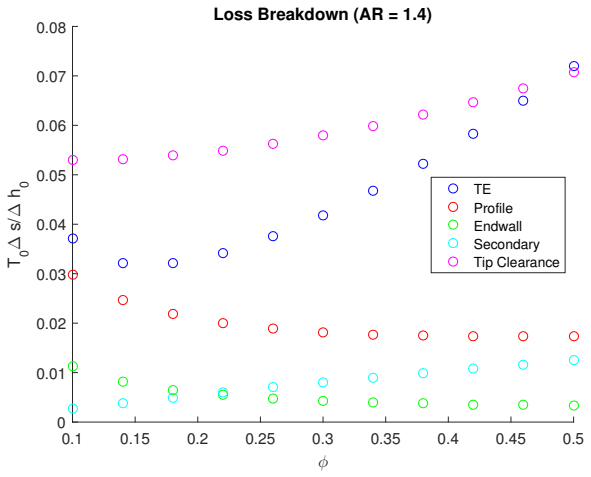

Figure 29: Lost Efficiency Breakdown and Variation

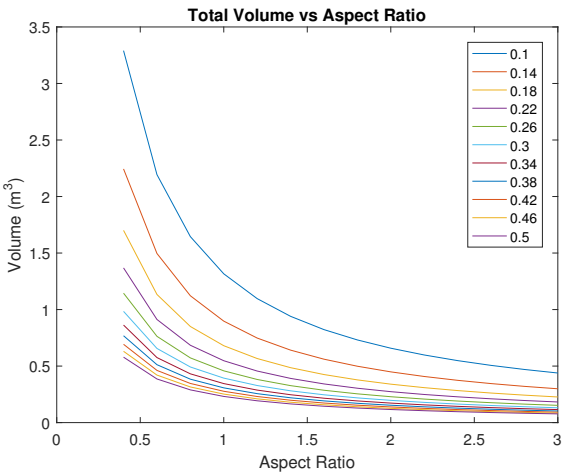

Figure 30: Volume Variation

The results obtained from varying ϕ also revealed an optimal value for the Flow Coefficient as approximately 0.23. Low ϕ resulted in high values for flow turning. This resulted in the decreasing relationship between ϕ and Profile losses (due to flow turning).

However the inverse relationship between Span and Flow Coefficient also results in increasing TE losses with ϕ. However the dependence of the TE Losses on the Profile Losses, especially acute at low Flow Coefficient results in an initially decreasing graph.

The combination of the variation of the different losses resulted in an optimal value of ϕ at 0.23.

5.4 Result Variation with Shrouded/Unshrouded Blades

For the following graphs $\phi = 0.4$, $n_{stages} = 12$ and $\psi = 2.4$.

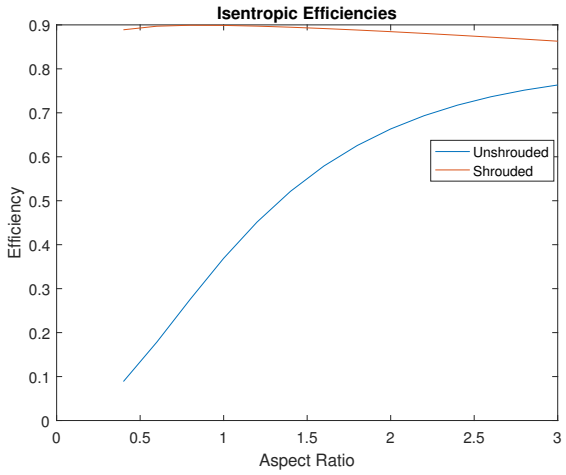

Figure 31: Maximum Efficiency Variation

The results highlight the importance of shrouded tips. Due to the small spans, the tip gap is a large enough relative to the span to result in significant improvements from having shrouded tips. Yoon et al 2010 [3], sets the break-even clearance below which unshrouded tips generate less loss than shrouded tips at 0.58% of the Span. All designs tested were significantly above the break-even clearance (the Span would have to be 20 cm for a 1mm gap and 10 cm for a 0.5mm gap).

6 Pareto Optimal Curves

Total turbine volume and Isentropic Total to total Efficiency were identified as the two main parameters that the client was interested in. It was therefore deemed necessary to evaluate the trade-off between both quantities, all other variables being optimised for the two quantities in question.

The resulting code allowed for ϕ, ψ, and AR to be floating. This resulted in a 4-dimensional matrix for the entropic losses. The overall efficiency and volume obtained by summing losses and individual volumes across the stages reduced this down to 3-D Matrices for the Isentropic efficiency and Volume each.

The 3D matrices were then flattened into two single-row vectors of the same length, while a new matrix of the same length was created to correctly store the corresponding flow parameters for the elements in the efficiency and volume arrays.

The arrays were then sifted through element by element. Two loops or counters were required. Every element in the array (tracked by the inner loop) with a larger volume AND lower efficiency that the reference element (tracked by the outer loop) was eliminated from the array. This resulted in a Pareto set for the volume and Efficiencies.

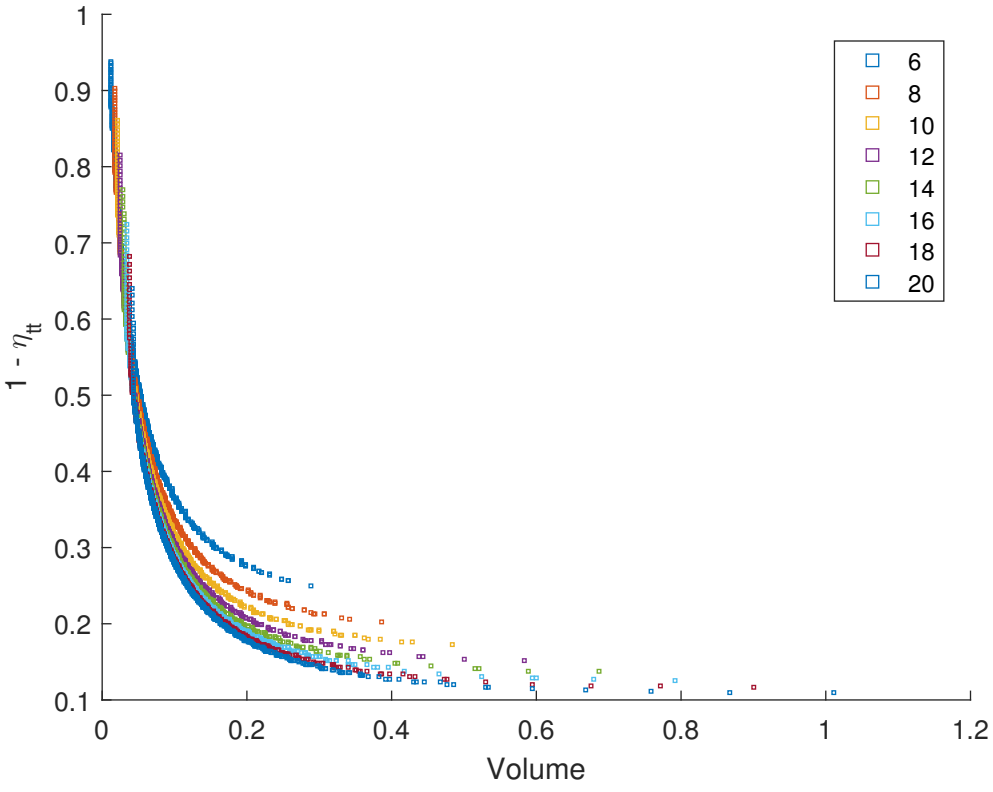

Figure 32: Pareto Curve Variation over n_{stages}, Gear Ratio = 1

The effect of varying the tip clearance could also be explored, and was found to be linearly related to the efficiency. This was expected from the linear relationship between the tip gap and fractional leakage flow (and consequently the entropy rise). To demonstrate the effect, the number of stages was set to 12 and the tip gap varied from $0.2mm$ to $1mm$.

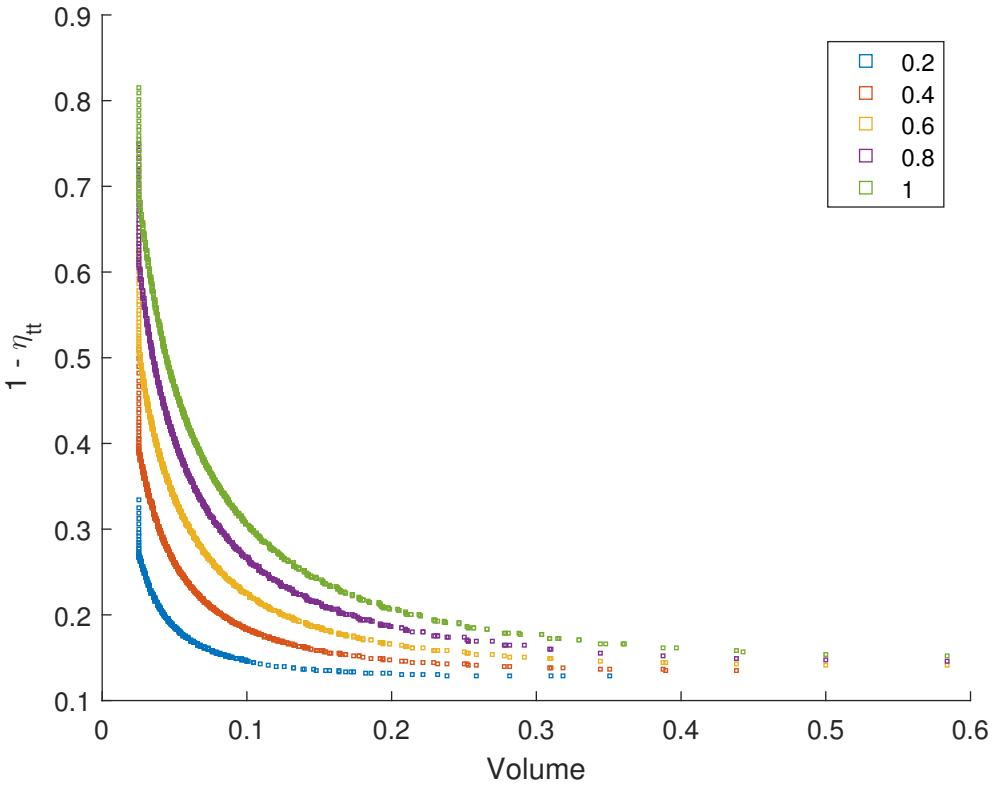

Figure 33: Pareto Curve Variation over t_{te}, $n_{stages} = 12$, Gear Ratio = 1

Since Trailing Edge Losses were so dominant, it was also thought necessary to explore the effect of varying trailing edge thickness. The curves were found to be quite sensitive to the Trailing Edge thickness, especially for low volume designs, which was expected, given the dominance of the TE losses for designs with short chords.

6.1 Mean-line Variation

The subsequent step in the analysis was to break away from the assumption of identical stages. Therefore, with the aim of maximising the suitability of stage span sizes to the work extracted per stage, the Δh_0 per stage was changed from being constant for all stages to a linearly increasing function over the turbine stages. The Isentropic enthalpy drop for the first stage was set at $0.5 \times \dot{w}/n_{stages}$, with the enthalpy drop per stage linearly rising to $1.5 \times \dot{w}/n_{stages}$ across the final stage.

There were multiple available methods to achieve the required enthalpy distribution. For the design modelled in this report, ϕ and ψ were fixed at constant values across all stages, with the Mean Radius and Axial Velocity increasing through the machine.

The Pareto Curves for the designs with non-constant mean radius have been plotted below.

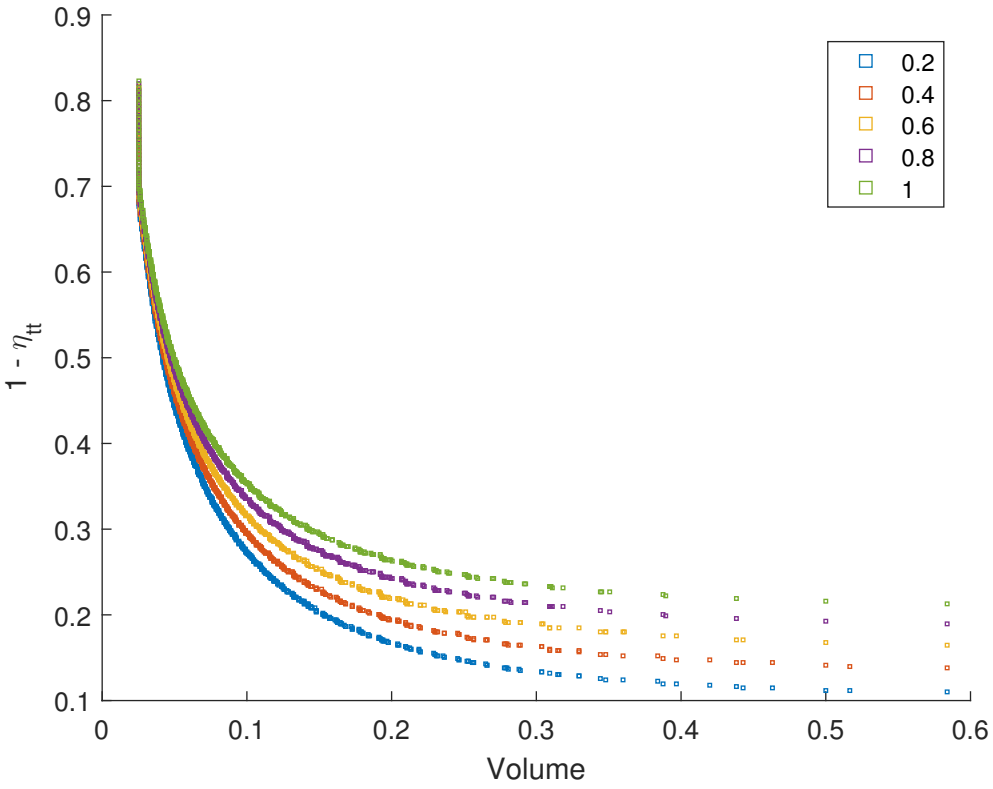

Figure 34: Pareto Curve Variation over Tip Clearance, Gear Ratio = 1

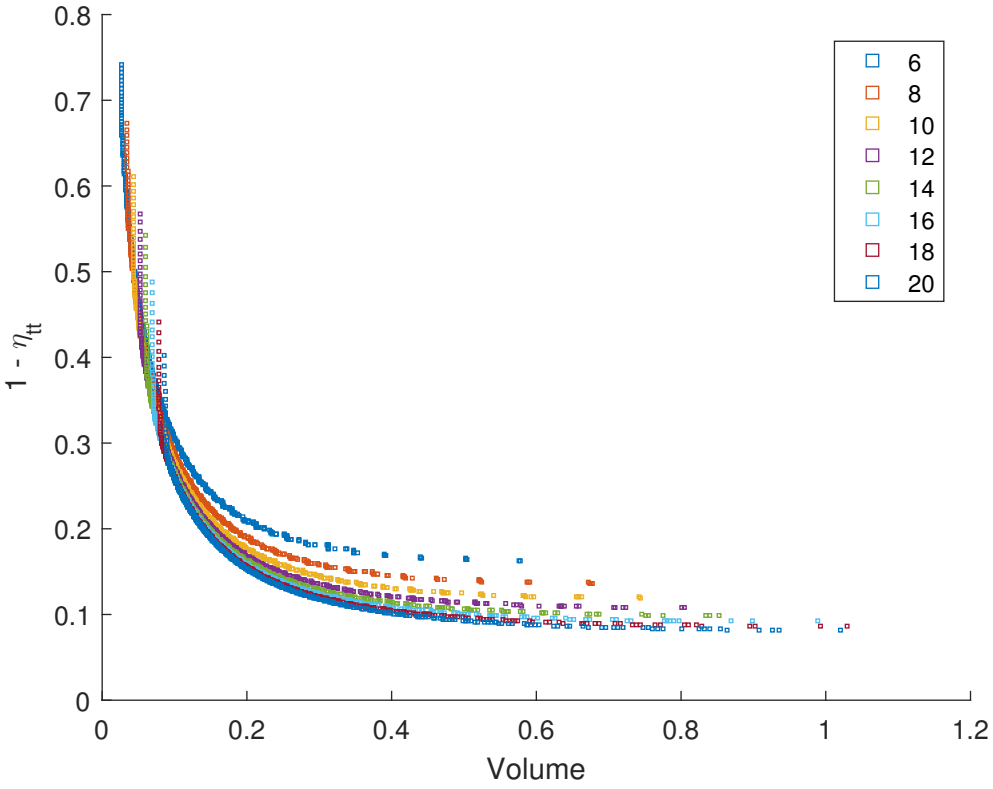

Figure 35: Pareto Curve Variation over n_{stages}, Gear Ratio = 1, Varying Mean Radius

Having non-identical stages in the manner described above results in an efficiency improvement across

the entire Pareto Set. The reduction in Δh_0 for the earlier stages, resulted in a lower required U, allowing for a reduced mean radius at these earlier stages and consequently allowing for considerably larger spans than with constant mean radius designs. This reduced nearly all losses (See Sec. 5), while slightly increasing the overall volume due to the increased radius towards the turbine exit.

7 Design Selection

7.1 Limiting Criteria

For selecting a candidate design, as the Pareto Curve indicated, a suitable balance between the volume and efficiency of the machine was to be decided upon. This was done by fixing the length at approx. 1.2m, with some flexibility to this requirement. The designs with the highest efficiency and lowest overall volume fulfilling this requirement were then explored. This placed the target design in a region around the 'corner' of the Pareto Curve. This was desirable as the corner region also represented designs with the most 'bang-for-your-buck' value; i.e the highest efficiencies without too much compromise on volume.

In addition to this, given the importance of the trailing edge thickness, especially in the 'corner' region of the Pareto Curves (See fig. 36), the design trailing thickness was reduced to 0.5 mm. This was considered a particularly crucial fabrication requirement since the length limitation placed most suitable designs close to the corner of their corresponding curve.

Further iteration of the the Pareto Optimization Algorithm indicated volume specific performance improvements up until n_{stages} 40,, beyond which efficiency gains around the desired operating region (on the curves) became negligible, and difficulty in fabrication increased in importance. The overlapping of the lower curves at volumes below $0.2m^3$ in Fig. 42 shows this.

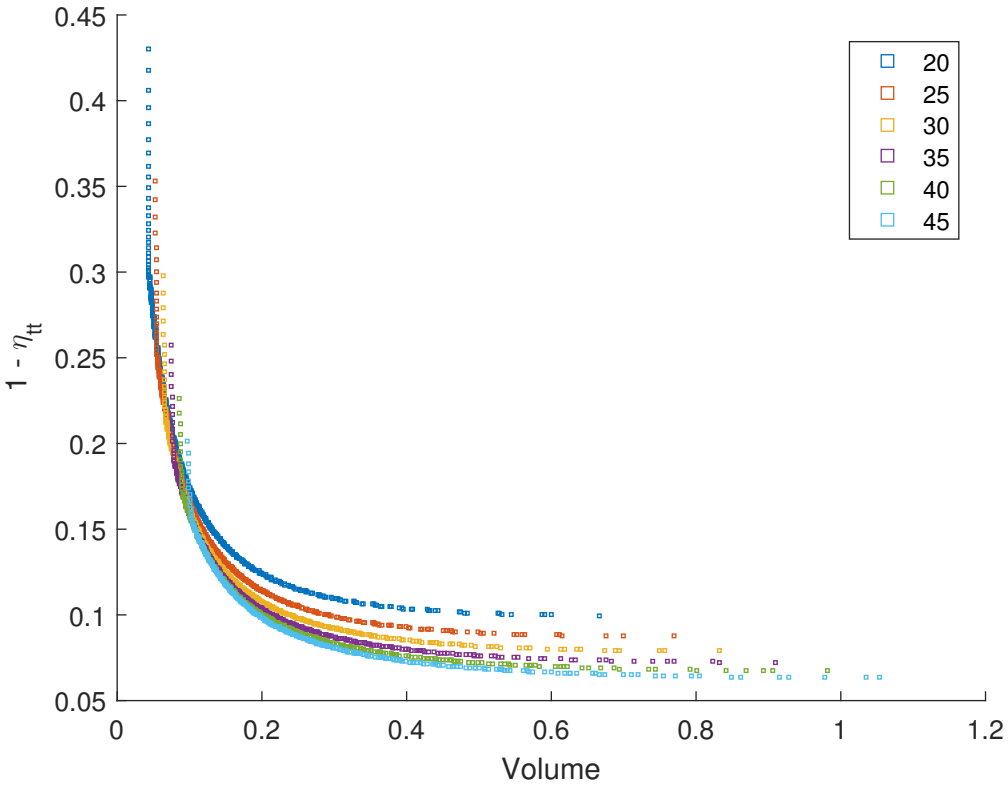

Figure 36: Pareto Curve Variation over $n_{stages} = 20 - 45$, Gear Ratio = 1

7.2 Effect of Adding a Gear Ratio

Counter rotation (equivalent to a Gear Ratio of 2) or adding a gearbox onto the turbine was expected to be of significant importance from the very outset of the design investigations. Increasing the effective rotation speed of the turbine would directly reduce the radius, and significantly increase the span across all stages, dramatically reducing the losses. For counter rotating designs the losses approximately halved for similar n_{stages}, with the marginal benefit reducing for higher Gear Ratios. Additionally, Gear Ratios above 3 suffered from excessively twisted blades ($r_{hub}/r_{tip} < 0.7$) and undesirably large centrifugal forces on the blades. The effect of adding a Gear Ratio to turbines with identical numbers of stages is depicted in Fig 43.

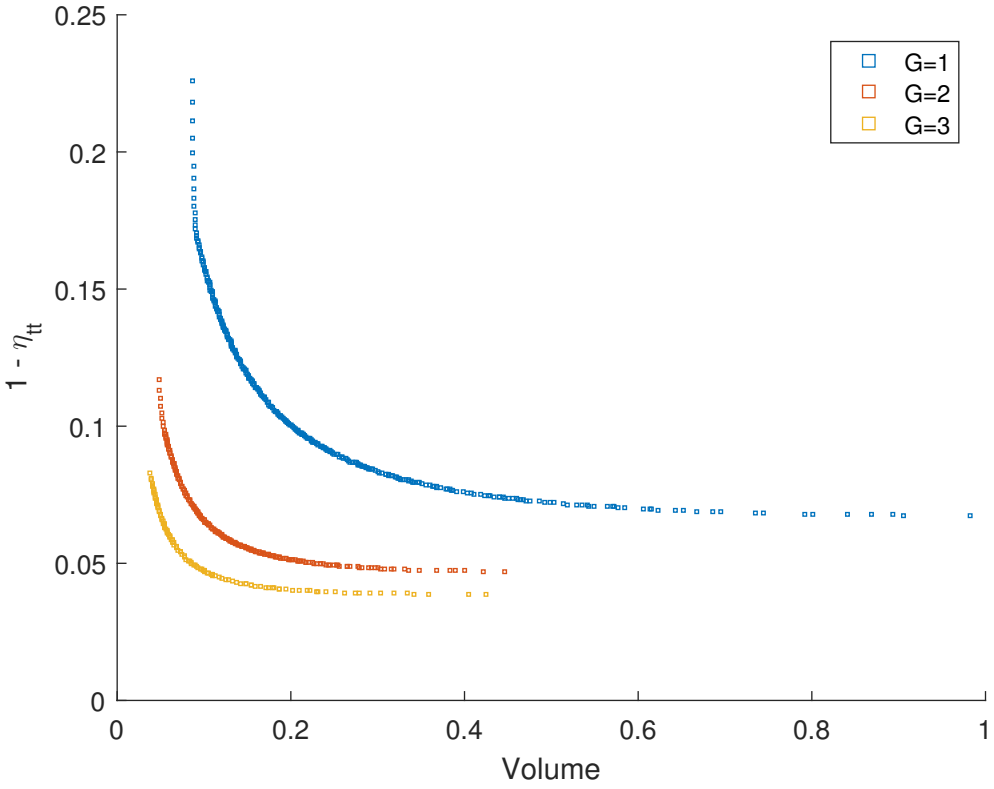

Figure 37: Pareto Curve Variation over Gear Ratios

While the dramatic loss reduction for machines with identical numbers of stages was unsurprising, a more interesting analysis examined the effect of adding a Gear Ratio G to machines with linearly scaled values of n_{stages}, i.e: 40 stages for G=1, 20 stages for G=2, 13 stages for G=3.

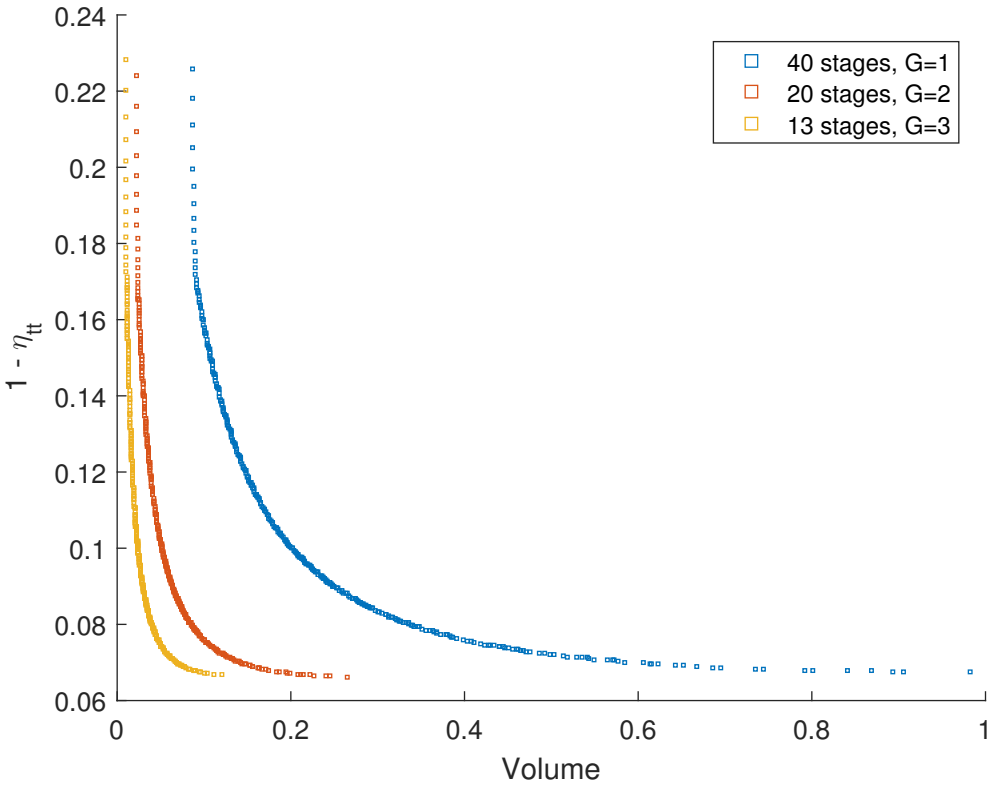

Figure 38: Pareto Curve Variation over Gear Ratios with adjusted n_{stages}

Fig 44 shows the remarkable improvement in efficiency for a given volume at even half the number of stages. It also shows the diminishing nature of the improvements with higher Gear Ratios.

7.3 The Effect of Non Identical Stages

The reasoning for having non identical stages and the chosen method to achieve this (i.e having an increasing Mean Radius, Axial Velocity with constant ϕ and ψ) has been covered previously. This section serves to compare machines with constant mean radii to similar machines with increasing mean radii (linearly increasing Δh_{0stage} as described in 6.1). Fig. 45 plots the resultant cumulative specific enthalpy drop across the turbine in both cases and Fig. 46 provides an explanation for the efficiency improvements by comparing the resultant Trailing Edge thickness to Throat width plots.

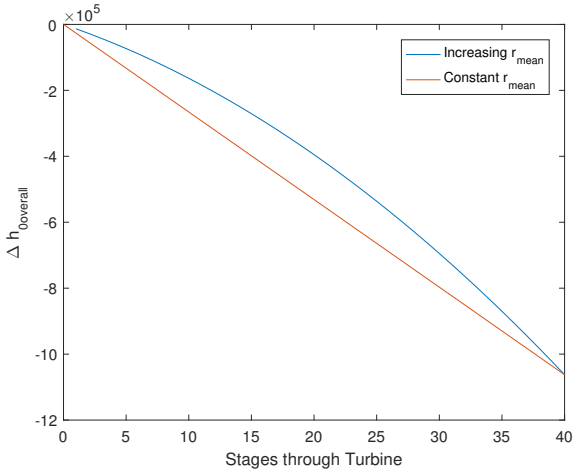

Figure 39: Enthalpy Drops (cumulative) through Turbine

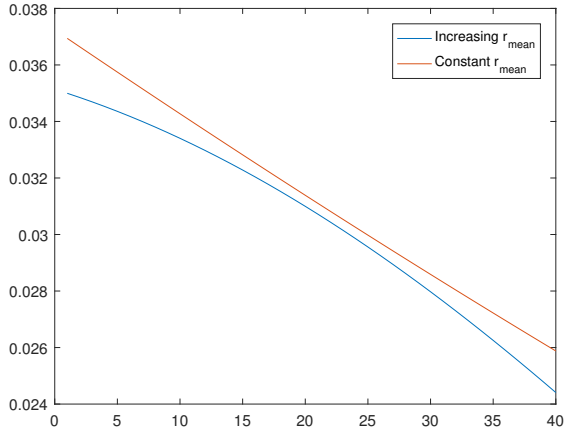

Figure 40: Trailing Edge Thickness to Throat Width Distributions through Turbine

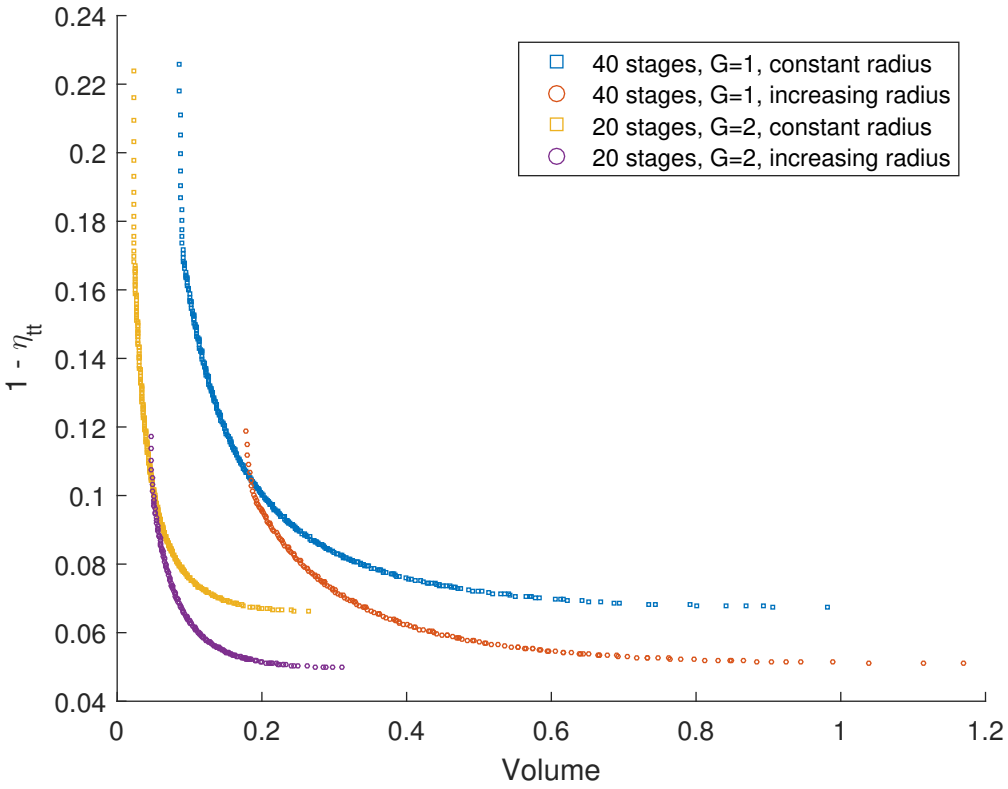

Figure 41: Pareto Curve Variation with constant and increasing Mean Radii

Fig 47 reveals that a flared mean radius resulted in higher volumes in the Pareto Set. However, crucially, it cannot explain if the volume increase for a given pair of points is due to an increased radius or length. The individual raw data sets had to be examined for this information.The figure interestingly reveals the increasing efficiency gain in having an increasing mean radius at higher values of G. The curves for both sets of Gear Ratios overlap at a certain minimum volume, with the increasing radius design having a noticeable efficiency advantage at volumes above this minimum volume. However, the minimum volume for a counter rotating turbine is lower than that for a normal rotating turbine, which. The self-imposed length requirement also set the target volume at approximately $0.19 - 0.2m^3$, and the efficiency advantage

for an increasing radius was considerably higher at this target volume for a counter rotating turbine than the advantage for a normal rotating turbine.

7.4 Axial Load and Pressure Vessel Thickness Calculations

A stage-by-stage Steady flow Momentum Equation (SFME) based calculation was carried out to find the net Axial Force on the turbine. The resulting formula was:

$$F_x = 2\pi r_2 \times (P_2 H_2) - 2\pi r_1 \times (P_1 H_1) - [P_{12} \times 2\pi (r_2 H_2 - r_1 H_1)] + \dot{m}(V_{x2} - V_{x1})$$

where '1' denotes quantities just upstream of the rotor, while '2' denotes quantities at the stage exit. The stagnation pressure at stage inlet and between the rotor and stator blade rows was assumed to be the same. P_{12} denotes the average pressure across the rotor blade row.

The Pressure Vessel thickness was calculated assuming the Tresca Yield criterion for a steel cylinder using the Stagnation Pressure at inlet.

7.5 Selected Designs

Based on the above investigations, the following table of candidate designs was compiled. For these designs, the tip gap and trailing edge thickness were both kept at 0.5 mm. The tip was also a shrouded tip.

	A	B	C	D	E	F	G
Gear Ratio	1	1	2	2	2	2	3
r_{mean} variation	Const.	Inc.	Inc.	Inc.	Const.	Inc.	Const.
n_{stages}	40	40	20	12	20	20	15
ϕ	0.475	0.875	0.825	0.225	0.25	0.3	0.275
ψ	1.15	1.25	1.2	0.9	0.9	0.8	0.95
AR	2.7	3	3	1.7	1.5	2.7	1.6
α_1^o	-8.97	-8.13	-6.91	12.52	11.3	18.43	5.19
α_2^o	66.16	52.12	53.13	76.67	75.25	71.56	74.28
Span (mm)	22.6-32.3	26.6-38.4	27.2-39.3	44.9-64.2	33.7-48.1	49.9-71.4	36.3-51.9
$r_{mean}(m)$	0.214	0.145-0.251	0.104-0.181	0.156-0.270	0.171	0.128-0.222	0.1282
Length (m)	1.2	1.24	0.8241	1.11	1.61	1.29	1.13
Volume (m^3)	0.1956	0.1964	0.0557	0.2208	0.1861	0.1855	0.079
$1-\eta$	10.17	9.67	9.10	6.44	6.74	5.21	6.34
Axial Load (kN)	141.14	176	125.95	247.7	149.26	236.09	121.3
Vessel $t(mm)$	9	9.4	6.5	9.9	7.6	8.5	6

8 Concluding Remarks

The overarching problem in designing the required turbine arises from the combination of a large work output that is needed to be extracted from a relatively small mass flow rate. As a result, the required blade speeds are very high. Adding this requirement to the finite shaft rotational speed results in a turbine with a large mean radius and consequently a very small span.

The small span results in a large tip clearance to span ratio, explaining the large magnitude and high

sensitivity of the results to the tip clearance. The small span also results in low values for the chord, pitch and throat width, resulting in unacceptably large values for the trailing edge to throat ratios. This is the primary driver for the Trailing Edge losses, by affecting the dominant 'blockage term' $(((t_{TE}+\delta^*)/w)^2)$.

Finally, the overall weight of the machine was to be considered. This was replaced with the more reliably calculable machine volume, with the assumption that the weight of the machine would scale approximately linearly with the volume. In addition to this, the required thickness of the Pressure Vessel holding the machine also played an important role, further specifying the fact that even among low volume designs, longer and 'thinner' designs were preferable.

Therefore, it was evident that efficient designs would seek to maximise the blade spans without affecting the overall machine volume too much.

8.1 Why have more stages?

Increasing the number of stages serves to reduce the enthalpy drop per stage. By having each stage perform less work while maintaining ψ, U, and consequently r_{mean} were reduced. This increases the span.

A similar argument can be made for flaring the mean radius. Having the early stages, where the fluid density is high and spans are comparatively small less loaded, the particularly lossy spans for the early stages can be increased (see fig. 46).

Increasing the number of stages to improve efficiency may seem counter-intuitive, since increasing the total number of blades, and therefore, the total number of trailing edge wakes, should increase losses. However, while the total number of blades does indeed increase with more stages, it does not do so by as large an amount as expected, nor does it increase linearly. This is because the number of blades per row decreases with more stages, which in turn benefits the trailing edge thickness to throat width ratio.

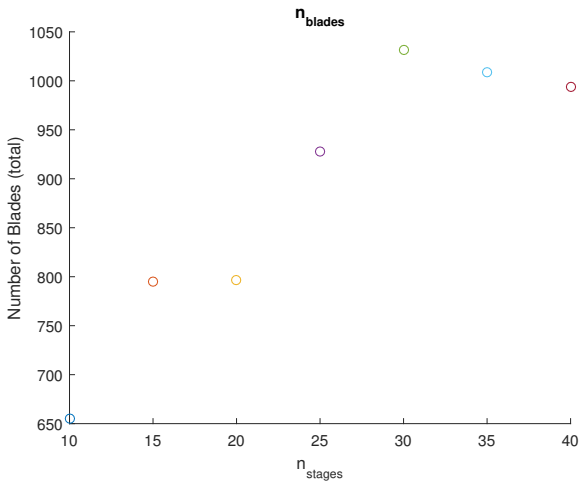

Figure 42: Total Number of Blades for different n_{stages}

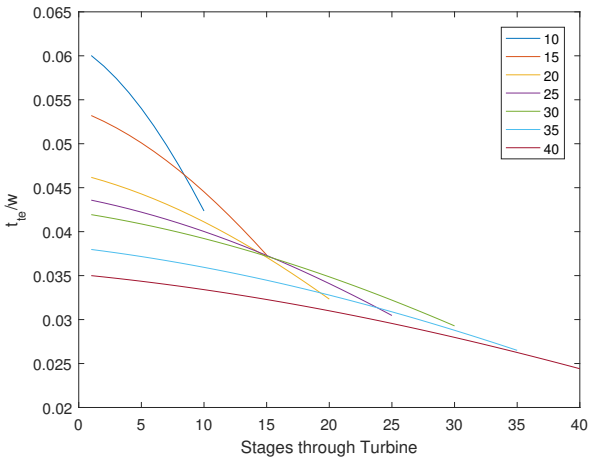

Figure 43: Trailing Edge Thickness to Throat width Distributions for various n_{stages}

8.2 Why Counter-Rotate?

Counter-rotation tackles the primary loss factor directly. Doubling the effective rotational speed halves the required radius, and therefore doubles the Span. In addition to dramatically reducing the losses, counter rotation also results in a volume reduction, due to the reduced radius. Therefore, even if the number of stages is halved, a counter rotating design, especially one operating in the 'corner' region of the Pareto

Curve, will be more efficient than a normal rotating design of the same volume. The reduced radius also results in a thinner pressure vessel to contain the turbine.

7.2 also details the diminishing returns from having a Gear Ratio higher than 2. The hub to tip ratio of these designs is also on the lower side and the high blade speeds can make blade stresses very large.

8.3 Conclusion

The modelling procedure reveals the sensitivity of the results to the tip clearance and the trailing edge thickness. It is therefore imperative that these two variables are minimized.

Increasing the number of stages increases the span (as explained earlier), which reduces the component of the losses from the tip clearance and trailing edge thickness by reducing the clearance to span and the trailing edge thickness to throat width ratios. The increase in volume due to the increase in length (from more stages) is also offset (to an extent) by the decrease in mean radius that increasing n_{stages} entails. This means that above a certain minimum volume, increasing n_{stages} increases efficiency at the same volume. It is therefore beneficial to have a high number of stages.

Counter-rotation provides significant benefits across the board with comparatively small drawbacks in the fabrication and losses associated with the fabrication. The efficiency benefits are large enough to offset difficulties in reducing the tip gap and trailing edge thickness.

References

[1] Denton, J.D., 1993, "Loss Mechanisms in Turbomachines"

[2] Denton, J.D., 2008, "Cambridge Turbomachinery Course, Vol 1, Axial Turbine Design"

[3] Yoon, S.; Curtis, E.; Denton,J.D.; Longley,J., 2010, "The Effect of Clearance on Shrouded and Unshrouded Turbines at Two Levels of Reaction"